S.I. : HIGH PRESSURE STRENGTH

On Thresholds for Dynamic Strength in Solids

N. K. Bourne[1]

Abstract

The limits of elastic behaviour change with the nature of the impulse applied to a target and the size of volume interrogated by a measurement, since it is the pre-existing defects sampled within its rise that determine the response observed. This review considers a range of solids of different material classes and tracks the development of the strength of the material during shock loading, from yield at the Hugoniot elastic limit, across the weak shock regime, to its transition to strong shock behaviour. It is shown that at this stress, the weak shock limit (WSL), the shear component of the applied stress exceeds the theoretical strength of the material. Beyond this threshold, there are a number of new responses that confirm a transition from an inhomogeneous to a homogeneous state. Further, whilst strength rises across the weak shock regime, it saturates at the WSL. For instance, failure in shocked glasses transitions from localised fracture initiated at target boundaries to a global failure at this threshold at the theoretical strength. Sapphire′s strength asymptotes to the theoretical strength of the strongest direction in its lattice. Finally, the fourth-power dependence of strain rate upon stress appears to be a consequence of the homogeneous flow in the strong shock regime. This review suggests that $\mu/2\pi$ is a good approximation for the unrelaxed theoretical strength of solids at increasing stresses beyond the WSL. The methodology unfolded here represents a new means to experimentally determine the ultimate shear strength of solids.

Keywords Strength · Shock · Yield · Threshold

Introduction

The strength of a target constructed from its constituent components is a vital measure to quantify its resistance to failure during loading, yet strength is a term which returns different levels according to the speed and severity with which one applies force. Science texts have derived a framework to classify the concept built over hundreds of years [1–3]. The discussion herein will show the strength of solids changing at different scales and across different regimes of applied, dynamic loading. There have been other reviews of strength measured during shock loading, but this focuses particularly on the transition in behaviour as one crosses from the weak to the strong shock regimes and beyond [4–13]. It will consider particularly compression states, and span the elastic regime, through to solids in states at the boundary with warm dense matter [10, 14–19]. In the lower stress regimes, the role of the initial distributions of defects in the as-received materials is key, and their significance across the boundary, between the so called weak and strong shock regimes, will be discussed in detail [4, 20].

The as-received microstructures of common engineering materials, and their states under ambient conditions, are the key consideration in the weak shock regime, where a wave loads material to a shear stress less than its theoretical strength. Thus metals, as well as brittle materials, polymers and composites, show a variety of behaviours in this regime [20, 21]. However, there is a thread that will be traced showing the behaviour of solids becoming ever more homogeneous as compression increases [18, 22]. In the weak shock regime, there is key dependence on the pre-existing defect structure encountered by the impulse since this leads to an inhomogeneous stress state seeded at these locations behind the front. In the strong shock regime dislocations are nucleated homogeneously at the front, which implies hydrodynamic flow behind the shock. Both these states are mediated by the effects of the increased temperature accessed as greater amplitudes of loading are delivered

✉ N. K. Bourne
neil.bourne@manchester.ac.uk

1   The University of Manchester at Harwell, Diamond Light
     Source, Harwell Campus, Didcot, Oxfordshire OX11 0DE,
     UK

[4, 23, 24]. It is hoped that the treatment presented here will draw together key features of response in a consistent manner across very different amplitudes of insult, to illustrate the role of applied stress thresholds in the behaviour of solids under shock loading.

Background

The effect of confining pressure on condensed matter has been a subject of active research and debate through the centuries [2, 20]. In particular there has been a focus on the failure of materials or structures under forces applied to the component or material in question [21]. The development of solid mechanics has created a framework in which dynamic loading leads to components of force decomposed into hydrostatic and deviatoric components and formal definitions of strength and criteria for damage were developed alongside these [1–3, 25]. Over time these concepts have been applied at smaller length scales and the increased strength of smaller and smaller components drives nanoscale research e.g. [26]. Thresholds delineate behaviour, beginning with measurements of the elastic/inelastic strains that fail a material.

The strain, and the strain rate (its speed of its application) are typically used as indicators that determine response to load. Here we will think in terms of the temporal components used to assign strain rate that may be divided into a time over which the impulse rises and a duration before it is released. These will be compared with the relaxation times for the operating micromechanics that accommodates the applied strain. Many solids are polycrystalline materials and, in more rapid loading, their response is governed by the transition from strain across the bulk to that within an individual grain as the applied pulse length decreases [6, 27]. Impact, laser-shock, explosives or electromagnetic pulses provide a suite of impulses of varying amplitudes and durations that excite phenomena at the fastest rates to overcome

strength within a material. In this respect, the shock is a critical tool that pumps a material within a particular loading envelope and probes a suite of mechanisms excited across the scales (Fig. 1). A range of techniques have been developed to analyse response and determine strength [28–33]. However, whilst an impulse appears to rise discontinuously at a longer timescale, at a lower one that rise will appear ramped. Nevertheless, ultimately it is the bonding within matter that mediates the strain induced and the mechanisms that operate.

There are two basic classes of structural response in crystalline solids considered here—the movement of planes down slip directions, and cleavage of interfaces in disordered or brittle materials. Of course, applying an impulsive load to matter will also trigger thermal effects and while some mediate the response observed, reaction may also be triggered within excited energetic materials. Planes in a deforming solid may slip past one another, or stacking may reorder by slight shifts in position in order to accommodate the displacements applied at an interface. As is well known, slip is mediated by dislocations in crystalline solids or alternatively twinning may occur if Peierls stress is high or where excess extra energy is required to insert a new atomic plane (see in [34] for example). In covalent materials, and in those where slip is difficult, cleavage is generally the preferred mechanism to induce the failure that accommodates strain [3, 34]. Finally, martensitic phase transformation, that operates with a very similar atomic movement to that induced in twinning, may occur in some solids as applied stress increases [5]. As stress amplitudes increase, more and more slip planes are activated to accommodate greater forces until eventually the crystal slips on every atomic plane at the point at which the shear strength of the material is overcome.

Fig. 1 The spatial scales in solids showing deformation mechanisms that operate to fail crystalline structures particularly in compression
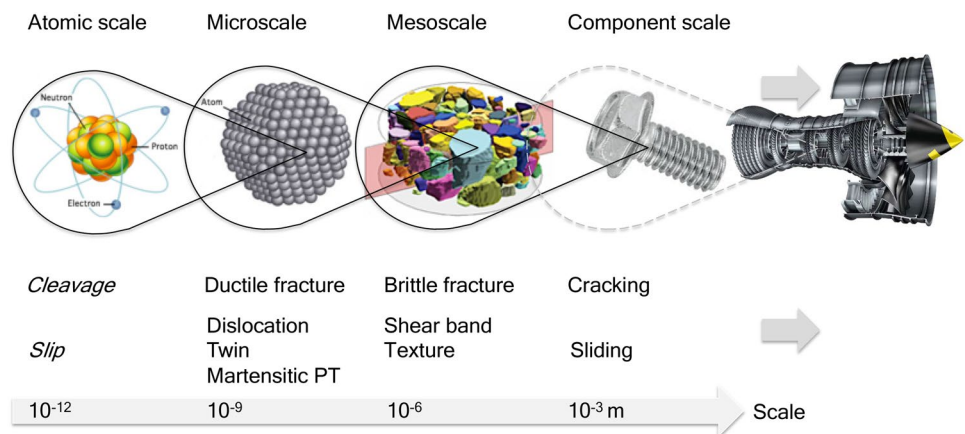
Strength in the Weak Shock Regime

Theoretical Strength

In compression, the yield strength refers to a limit beyond which the valence electronic shear strength is exceeded and the solid adopts a new stable electronic conformation [35, 36]. Of course, such strength approaches a theoretical limit as the volume of material considered shrinks to atomic dimensions [37, 38]. Discussion of how to determine this theoretical strength began with the work of Frenkel and Orowan-Polanyi, and has been extended and made more accurate over the years [26, 39–44]. Whilst there is still no agreed method to measure the theoretical shear strength, it may be determined by a range of methods of increasing computational complexity, particularly now that ab initio methods are routinely used to determine values for particular slip systems in ideal lattices of ionic or covalent crystals [45–47]. The theoretical shear strength for a material (τ_{Th}) may be estimated analytically using a range of methods, but one simple and powerful approximation, after Frenkel, is given by the shear modulus $\mu/2\pi$ [26, 41, 42]. This value is used in what follows but is, of course, an approximation. Other workers have calculated values for the ideal shear strength in the range $\mu/18$–$\mu/4\pi$ using ab initio calculations deforming unconstrained crystals to failure [48–50]. This range has been shown to be consistent with nano-indentation data (indenter 50–1000 nm) in the metals Al and Ni [51]. However, these calculated values correspond to the fully relaxed state although other calculations also show that lattices have an energy of order twice this magnitude giving a calculated shear strength close to $\mu/2\pi$ [49, 52]. Thus, in what follows, this latter value will be adopted as a representative value for the theoretical shear strength in the *shocked* state.

Yield Strength and Tensile Strength

Investigation over many years has shown yield strength to increase with strain rate. This means of framing the problem has served macroscale engineering problems well. However, the strength at failure is never more than a fraction of the theoretical strength because of pre-existing stacking and volume defects. The Hugoniot elastic limit (HEL) is the yield stress in one-dimensional strain for a solid. Polycrystalline materials are generally composed of grains of random orientation with amorphous or low order regions between them and thus, in the general case, appear isotropic beyond the mesoscale unless worked or alloyed to achieve a particular texture. These observations are represented mathematically in constitutive descriptions of materials typically used in macroscale simulations of engineering structures under load [6, 53]. More complex behaviour is found for anisotropic

materials, for instance the triclinic α-alumina (sapphire) crystal that shows a range of HELs between r axis *ca.* 12 and c axis, 21 GPa [54]. In contrast, the alumina AD995, that consists of a polycrystalline composite of these crystals with random orientation, has an HEL of 6.7 GPa which is much less than that for the loading in 1D down the weakest direction. It can however plastically yield down easy directions in a 3D strain state at the mesoscale in this composite and recovery of shocked AD995 shows the onset of twinning in suitably oriented grains at this stress [55]. It is this first yield in the composite that bounds a region of mixed response where some grains behind the shock are still not plastically yielding up to the point where the shock amplitude exceeds the yield stress down the c direction. We shall return to higher amplitude loading of this alumina in section 'Strength in the Strong Shock Regime' below.

There is a volume of pre-existing defects typically found within solids at the mesoscale that sets the boundary for the deformation that follows when it is shocked [34]. In rapid loading, dislocations or tensile failure paths are generated behind shock pulses. Dislocation theory provides examples illustrating these including Frank-Read sources in FCC metals at lower strain rates for instance, moving to homogeneous nucleation at strain rates greater than 10^7 s^{-1} [48, 61, 62]. If pulses are applied slowly, plasticity is stabilised around these pre-existing defect sites since the strain fields around them remain uniform; if pulses are longer in duration then the volume across which the applied strain is distributed is larger. Those that are faster rising sample smaller volumes and thus sweep fewer pre-existing defect sites as they propagate. Thus, failure is pushed to higher load amplitudes. This is illustrated in Fig. 2, which shows measurements of compressive and tensile strengths in planar shock experiments; longer, more slowly rising pulses induced by flyer plates and shorter, rapidly rising ones induced by lasers. In both cases the metal loaded is pure, (FCC) aluminium—one of the standards investigated in dynamic experiments [23, 56, 58, 63–69]. The pulse lengths are limited by the loading methods and sample geometries adopted. In Fig. 2a. the magnitude of the elastic precursor (the Hugoniot elastic limit; HEL) is measured for different pulse loadings on pure aluminium films and shows an increase in measured compressive strength with decreasing pulse length. In Fig. 2b, the spall strength of the foil is shown and as loading time reduces, the tensile strength again increases.

Of course, as the duration and the risetime of the pulse are reduced, there is a corresponding decrease in the target volume sampled and thus the number of pre-existing defects within the microstructure that are accessed. This fails the material at higher stress levels and results in increased shear and tensile strengths measured in the target. There are two manufacturing routes for the aluminium targets in each class of experiment; rolled sheets in the case of the plate impact

Fig. 2 Aluminium elastic limit and spall strength as a function of load time. **a** Compression experiments [56, 57]. **b** Tensile experiments conducted using plate impact and laser loadings [58–60]
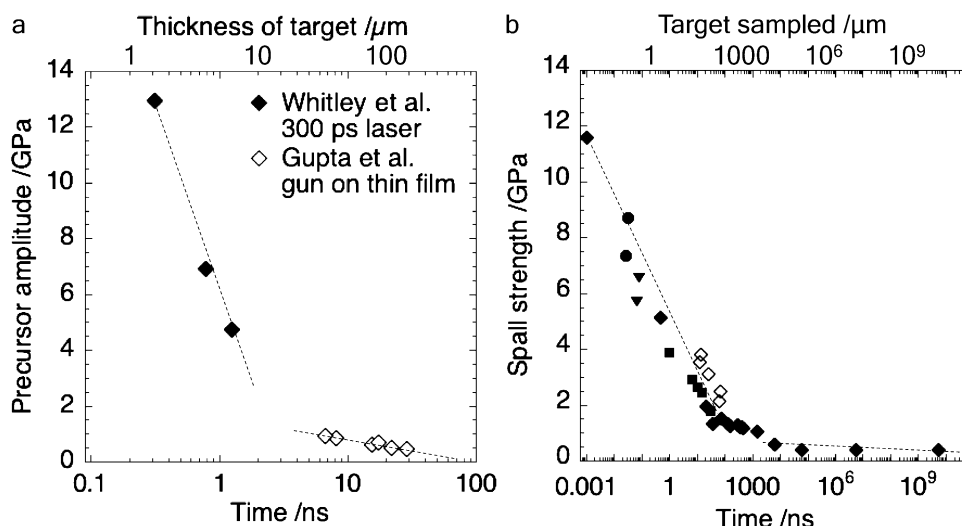
experiments or vapour deposited films for those in the laser loading. Both of these present a different defect population to each respective impulse, although the experimental measurements acquired will integrate a distribution of responses to each [21, 34]. In both cases the strengths recorded asymptote to higher values ultimately reaching the stress at which the theoretical strength is reached for pure aluminium which is *ca.* 18 GPa derived using the approximation (5) described below.

There is a critical threshold in behaviour crossed between *ca.* 1 (compression) and 10 ns (tension) (*ca.* 10 μm) and this corresponds to the confinement of the changing state of strain within grains. Here the pulse risetime samples a number of inclusions and stacking defects alone without failing additional grain boundaries or second phases of lower strength [4, 20, 21, 28]. This corresponds to a critical strain rate at which measured yield strength is seen to rise rapidly and which, for aluminium, is *ca.* 10^6–10^7 s^{-1}. Other authors have discussed transition to a phonon drag mechanism at this stress [70]. In spall, failure occurs by interactions that supply a dispersive tensile impulse and so this region is somewhat wider. Nevertheless, this rapid loading filters many of the failure mechanisms that might occur at defects at larger scale and renders the material to appear stronger as a result. Inertial confinement ensures that the volumes accessed become sufficiently small that the loading period of interest has been probed before the presence of boundaries can relieve the strain and in shock loading this region confines the strain to be uniaxial at the macroscale [4, 21].

Related behaviour is seen in other FCC metals such as copper or nickel, which also harden with strain rate as dislocations entangle during rapid loading, whilst in BCC tantalum, strength increases with strain rate *without* hardening on unloading since the Peierls stress is much higher and the nucleated dislocation density much lower [21, 28,

29, 31, 33, 53, 71–75]. Ceramics show a similar behaviour, with strength remaining constant as loading pulse length decreases, until the rise of the load no longer probes the weaker glass matrix and starts to purely strain the hard crystals contained [76–81]. Finally, in polymers, strength rises as the pulse probes smaller, cross-linked sectors (such as spherulite structures for thermoplastics) [82–92]. It is clear that the scale of the volumes probed in matter, the times taken for mechanisms to complete, and the magnitude of the disturbance applied, all have a marked effect on the responses observed. The microscale/mesoscale boundary is a critical length scale where behaviour in metals, for instance, transits from polycrystalline texture to periodic order and this is reflected in response at high strain rate in materials under load. In both cases the strengths recorded asymptote to the theoretical strength of aluminium which, calculated using the formalism described below, is *ca.* 18 GPa.

Compressibility

There are thresholds in compressive behaviour that, when applied to a pulse, open up new modes of response for a microstructure [14, 16, 17]. The elastic-inelastic transition is the first of these accessed as stress amplitude increases. Beyond this stress, crystalline solids inelastically deform at stacking and volume defects that trigger slip, twinning or fracture in materials [34]. However, in the region above the elastic limit, most materials deform by processes that compress it to a more homogeneous state. First order, martensitic phase transformations may occur at higher stress levels and melting or other transformations at higher pressures again [5, 23, 93–95]. However, until the theoretical strength of the material has been exceeded, volume defects, present initially in the material for instance, have not been eliminated and

there are still inhomogeneous states behind the front. There comes a stress level however, at which the processes triggered are driven sufficiently quickly that they complete in a single front travelling faster than the elastic wave-speed

over the years and several sources for these are archived in a series of key sources [97–99]. These show that the shock velocity, U_s, typically shows a linear relation as a function of the particle velocity, u_p, thus

$$U_s = c_0 + S u_p \text{ where } U_s \text{ is shock front speed, } u_p \text{ the particle velocity behind it and } U_s = c_L \text{ at the WSL} \qquad (1)$$

within the material. Above this threshold, the front separates virgin from homogeneously deformed material and the width of the front, representing the time to complete these

The overdrive stress, the longitudinal stress, σ_{WSL}, that has a shear component corresponding to the theoretical strength, τ_{Th}, is given by

$$\sigma_{WSL} = \rho c_L u_p \text{ where } c_L = U_s, \text{ which from (1) implies } u_p = (c_L - c_0)/S. \qquad (2)$$

processes, decreases monotonically with increasing applied stress level [96].

The point at which this overdrive occurs represents the end of weak shock behaviour and defines the weak shock

An approximation can be made for isotropic materials, assuming a simple Tresca yield criterion, to relate the strength in one dimensional strain (the HEL) to the shear strength at this stress through

$$\sigma_{HEL} = 2(1-v)/(1-2v)\, \tau_{HEL} \text{ where } \tau_{HEL} \text{ is the strength at the HEL and } v \text{ is the Poisson's ratio in the ambient state.} \qquad (3)$$

limit (WSL). At this point the shear component of the stress applied exceeds the theoretical strength of the material. A

The ratio α between the yield and shear stresses will be used to connect elastic stress and shear states where

$$\alpha = 2(1-v)/(1-2v) \text{ and thus } \sigma_{WSL} = \alpha \tau_{Th} \text{ may be used to calculate the WSL.} \qquad (4)$$

single shock drives at a velocity U_s and overtakes the elastic precursor so that the shock speed is equal to longitudinal wave speed, c_L, to overdrive the material of initial density, ρ, Fig. 3a [24]. Compendia of data gathered in shock compression measurements on many solids have been collected

There are various means to calculate or deduce a value for the shear modulus of solids and this value can be converted to a longitudinal stress equivalent by using (3). For instance, it is possible to deduce the ambient shear
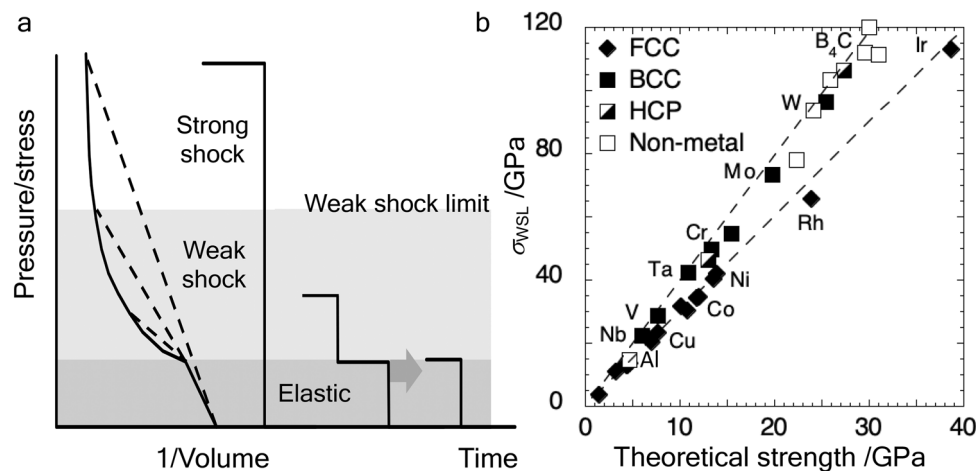
Fig. 3 a The weak shock and strong shock states and over drive; an elastic pulse at lower stress levels shows two waves once yield occurs and inelastic processes take time to complete. At higher shock amplitudes the shock front travels faster than the elastic wave and above a critical stress, a single shock front is driven into the target. This threshold is the weak shock limit (WSL) and divides strong and weak shock behaviours. **b** WSL versus theoretical shear strength for a range of material and elements taken from data published in the collections [97–99]. The two straight lines represent the factor α in the elastic relation (Eq. 4) for the two values of Poisson's ratio of and ¼

modulus μ of the material, by ultrasonically measuring shear wave speeds, c_s, in as-received samples under ambient conditions. This measurement can be used to deduce a theoretical strength through $\mu/2\pi$ where

$$\mu = \rho c_s^2 \text{ and thus } \tau_{Th} = \rho c_s^2/2\pi. \tag{5}$$

thus, values for the elastic stress corresponding to the theoretical strength can be calculated since the weak shock limit corresponds to the elastic limit of a defect free material. Values for the WSL can thus be recovered in several manners and these will be used as a framework to discuss the strength limits in a range of materials at the transition from weak to strong shock behaviour. However, it should be noted that the yield criteria (3) is an approximation first since it uses mechanics derived for a macroscale response and secondly since it assumes isotropy which is a reasonable approximation for polycrystalline, ductile metals at the macroscale but not for the anisotropic materials. The equation $\sigma_{WSL} = \alpha\,\tau_{Th}$ is consistent with the compendium of shock measurements examined for realistic values of a across all of the data so far reviewed by the author.

Strength in the Strong Shock Regime

Figure 3 shows the theoretical shear strength correlated with the observed limit of weak shock behaviour across a range of materials. This regime is dominated by valence electron bond strength. Inner core electron interactions are only seen at a much higher threshold where compressions exceed several hundred GPa; this region will not be considered further in this paper. The stress corresponding to the theoretical strength, σ_{WSL}, is equal to $\alpha\tau_{Th}$ (Eq. 4), where the factor α depends upon the initial, ambient properties of the element sampled. As discussed, the relations derived above apply to isotropic materials with no assumptions made about

microstructure, however, it is nevertheless remarkable that clear trends are observed in mapping Hugoniot data for a great range of materials.

Of course the WSL has a numerical value greater than the theoretical strength, and at least for the elements listed in [24], lies between two extremes determined by structure (Fig. 3b). The data for these curves are largely taken from shock experiments and were gathered in the post war period [97–99]. The two dotted lines bound the data and represent the ratio α, through Eq. (4), using values for the Poisson's ratio of 1/3 and 1/4, typical of ductile and brittle materials. It is clear that BCC and covalent materials lie on a different trajectory to their more densely structured FCC counterparts even though their initial Poisson's ratio is close to 1/3, whilst others lie in states between these two limits. Despite the uncertainties in calculating theoretical strength by this treatment, these trends are clear, and there are indications both here and in other work that Poisson's ratio retains importance beyond the elastic limit. This indicates that the behaviour of materials in the weak shock regime is not fully hydrodynamic reflected in changes in the Poisson's ratio until the WSL is reached [100].

Above the WSL, inhomogeneous states are confined to the zone spanned by the shock rise. States behind the shock are inhomogeneous in the weak shock region. Processes within the front have been discussed extensively by Grady in his work on the structure of shock waves. He has shown that in the strong shock regime, the strain rate in the pulse is proportional to the shock amplitude to the power four, $\dot{\varepsilon} \propto \sigma^4$, and has discussed the energy balances inside the front that lie behind this relationship [96, 101, 102]. At lower stresses, lower powers are recovered. Again, this indicates that the equilibration of inhomogeneous states takes a time which has a strong dependence on the stress level attained. In crystalline systems, slip processes transit from activation of slower, pre-existing dislocations and new loops created by Frank–Read sources for instance, to homogeneous

Fig. 4 Transition from weak to strong shock behaviour in silicates. **a** Streak sequence showing shock driven by impact of a thick copper flyer plate onto soda-lime glass impact at 500 m s^{-1} inducing an elastic stress of 5 GPa. **b** U_s-u_p for soda-lime glass and quartz [97, 98, 104]
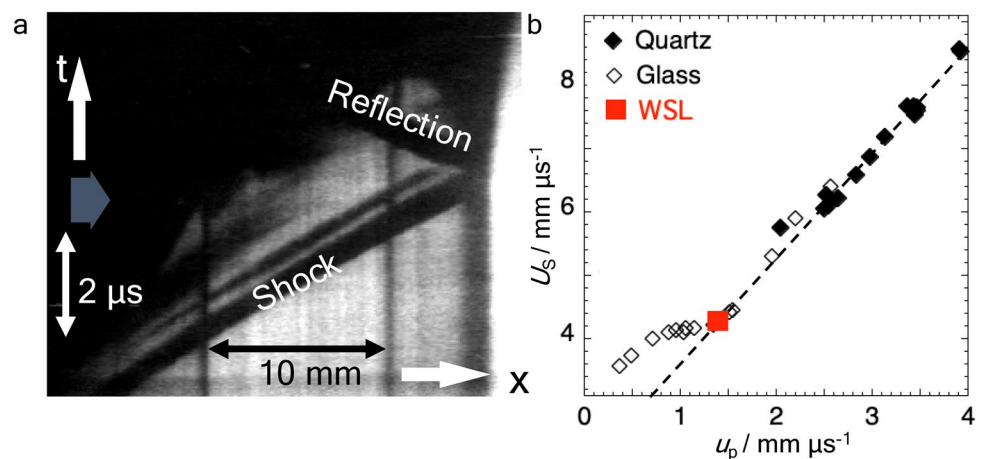
nucleation above their theoretical shear strength [103]. The transition will be explored in brittle systems below.

Quartz and glasses are both important natural and engineering materials and also illustrate a suite of densification mechanisms that complete at the weak shock transition in strong, covalent brittle solids [105, 106]. Two sources of data for quartz and for the more open structure soda-lime (SL) glass are combined in Fig. 4 [76, 97, 98, 107]. At lower loading amplitudes, the processes operating in the inhomogeneous region between the elastic and shock fronts are easily seen since glass is transparent. Failure waves are phenomena by which glass is seen to densify, and a fracture front lags behind a pseudo-elastic shock travelling ahead of it [78, 106–110]. Figure 4a shows a streak sequence taken after the deformation of soda-lime glass shocked to a stress of *ca.* 5 GPa. Impact induces an elastic front that progresses across the target and reaches the free surface after *ca.* 3.5 μs. As it reflects, the interface is accelerated, and darkened areas show decompression at the free rear surface. Further, a slower, dark fracture front propagates back towards the impact face behind the release. Two vertical lines are ruled onto the far surface of the target to fix a spatial scale for the sequence. Viewed through the compressing glass, these are refracted and deflected by the moving front and compressed material behind both shock and release indicate that both the refractive index and the Poisson's ratio, *v*, are changing [100, 108, 109, 111].

The first front travels at a velocity which settles to an elastic wave speed but is initially some 20% slower than this. This unsteady behaviour is also observed in sapphire in the weak shock region. Further, the shock rise (and thus its width) broadens with travel distance. There is a second, parallel region seen following the shock, which denotes a relaxation in stress behind the front that is seen here since schlieren imaging displays regions of changing compression. The failure front, which is believed to be fracture, follows at a slower speed (around 2 mm μs^{-1}), *ca.* half of the shear wave speed at this stress level. The imaging of a transparent material gives detail not normally directly observable, showing incubation times and details of operating mechanisms in the compression of this partially filled glass. As the amplitude of the impulse becomes greater, failure mechanisms become overdriven and the dark front is seen to merge into the shock.

Above the stress amplitude at which all deformation is within a single front, the value of U_S increases linearly with u_p and the compression of the open-structured glass follows the same path as the quartz single crystal data seen in Fig. 4b. There is a clear transition here to a linear behaviour (indicated by the dotted line) and at a stress of *ca.* 14 GPa the open-structured glass compresses and assumes the same trajectory as that of crystalline quartz. Interestingly, both diamond anvil and shock compression experiments on quartz and glass have shown changes in refractive index and in the Poisson's ratio as pressure increases, and these appear to saturate at *ca.* 14 GPa [108, 111–115]. At this value, densification processes are complete in the open structured glass as verified by several independent classes of measurement and both SL and quartz share the same values of c_0, S and of course the same Poisson's ratio (that of the quartz). Calculating the value of the WSL for both silicates
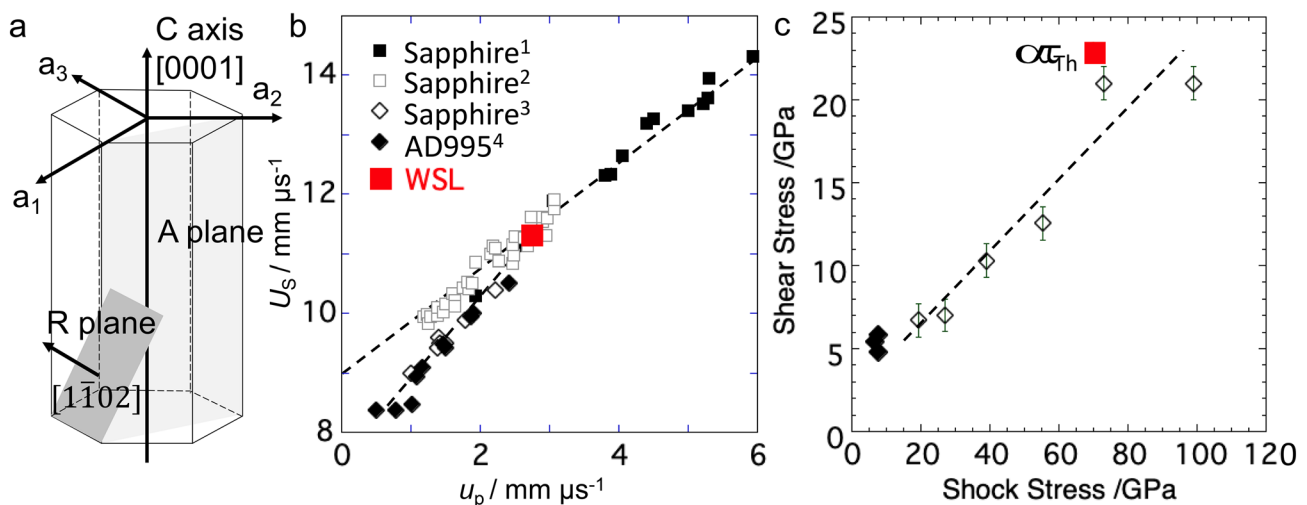
Fig. 5 **a** α-Alumina unit cell. Note two directions of note for this work—the highest strengths loaded down [0001] and the weakest down [1 1 0 2]. **b** U_s-u_p data for AD995 and *c* cut sapphire, the red square represents the WSL for *c* cut ($U_s = c_L$); data from [1][123], [2][98], [3][124], [4][119]. **c** Shear stress as a function of shock stress; data from [55, 119, 124]. The black diamonds represent the strength calculated from the measured AD995 HELs. The open diamonds show measured data for AD995 and indicate strengthening of the composite. The red square represents the WSL for the sapphire *r* direction [23] (Color figure online)

in the manner indicated above shows a common value of 14 GPa. Of course, whilst Poisson's ratio has changed for the open structured glass as pressure has increased, this will also occur beyond the WSL. This behaviour has analogies for all classes of metal, brittle and covalent materials loaded by shock as the reader will appreciate [79, 116–122].

An analogous behaviour is observed in aluminas and sapphire as their strength evolves while impact stress increases. Figure 5a shows the unit cell with assignments of key structural planes and normal directions. Loading down the c direction has the greatest resistance to shear whilst that down r or n planes (which are $ca.$ 60° to the c axis) shows the lowest. At first yield, it has been noted that single crystal sapphire (density 3.989 g cm^{-3}) shows HELs in the range 12–21 GPa [54]. The response to shock down seven directions of the α-alumina unit cell has been studied by Kanel et al. who noted the complex evolution of the loading history of the material and the steadiness of the wave up to 86 GPa [121]. The behaviour in this regime is dominated by unsteady waves and elastic precursor decay evident down all loading directions. Like the glass described above, the elastic front does not settle to a steady value for some run distance, which suggests that shear strength is developing in this region as suggested previously by Duvall [125]. The alumina AD995 shows composite behaviour. The quoted value for the HEL (6.7 GPa) represents a lower limit for plasticity within favourably oriented crystals down the r direction and twinning is observed in some grains of the shock-recovered composite microstructure above this stress level as noted above [55].

The shock velocity-particle velocity data illustrate the change in behaviour at the upper limit of elastic behaviour—the WSL (Fig. 5b). Data is presented from a series of investigations of single crystal and (composite) alumina AD995 [98, 119, 123, 124]. The data presented follow a scatter of trajectories below the value of the WSL ($U_s = c_L = 11.26$ mm μs^{-1}). This corresponds to a WSL stress of 123 GPa calculated from (2). This scatter in values of the constant S reflects compressibility changes with pressure down the different loading directions which is manifested in the unsteady wave propagation discussed above. Above the WSL however the material is in a homogeneous state and settles to a single curve.

The measured strengths are shown in Fig. 5c and follow a monotonic rise until $ca.$ 70 GPa [55, 119, 124]. Ultrasonic measurements and calculations of the shear modulus of α-alumina down different directions give values between 145 and 175 GPa. These shear moduli reflect the unit cell, with the highest values for shock recorded for loading down the c axis [0001] but easier shear down planes down the r direction [1 1 02]. The alumina AD995 again provides an interesting test case, containing a range

of crystals arranged with random orientation to the applied shock. The measured strengths for AD995 rise from the measured elastic strength at the HEL of $ca.$ 5 GPa to a peak of $ca.$ 21 GPa [124]. This compares with the calculated value of the theoretical strength for the r direction of 23 GPa which, using (3), implies a WSL of 70 GPa (red symbol on figure). The theoretical strength in the c direction is 31 GPa at a WSL stress of $ca.$ 123 GPa as seen above. Interestingly this lies in the range within which Urtiew observed shock-compressed sapphire to lose transparency in the infrared [126]. More recently, the electrical resistivity of shocked sapphire was found to begin to decrease significantly with increasing shock pressures above 130 GPa, which adds weight to these observations [127].

Discussion

The limit of elastic behaviour defines a point at which defects already present within a sample seed deformation during loading when further activated by a shock wave. In macroscopic experiments, this defines the stress threshold beyond which inelastic work is first possible. The loading impulse further determines the regions sampled and filters the mechanisms that can operate there. Strain rates of 10^5–10^6 imply sampled volumes of tens of microns in dimension within the rising front. Typically, a 2 μs pulse loads a $ca.$ 10 μm volume which cannot be released on the timescales of classical shock experiments and thus fixes uniaxial strain conditions at the macroscale at least.

The typical operating deformation mechanisms in inert materials include slip, fracture, twinning and martensitic phase transformation. The latter two processes occur quickly, with motion of only half an atomic spacing necessary to move planes past one another. Nonetheless they still result in fixed strain increments. To apply greater deformation to a material requires slip or fracture and these processes tend to operate more slowly and continue for as long as a driver is maintained. As stresses get higher, or the volume loaded in the rise of the pulse gets smaller, the theoretical strength of the material is approached. This can be seen in the experiments of Fig. 2 above. These observations suggest that the scale of the region in which loading is applied should be included into the constitutive description of the material explicitly if the observed behaviours are to be modelled with fidelity.

As loading pulses of higher amplitudes are applied, the theoretical strength is eventually exceeded, pre-existing volume defects are closed, and work is done homogeneously nucleating dislocations and heating uniformly across the front. The transition to a homogeneous state, at the weak

shock limit, requires all operating deformation mechanisms to complete within a single front. This may be seen directly in glasses (Fig. 4) where delay of inelastic processes at lower stresses accelerates into a single front at higher. Since failure processes can be simultaneously sensed and visualised, operating mechanisms can be identified. These observations in a range of materials where shock data exists, suggest that $\mu/2\pi$ is a good approximation for the unrelaxed theoretical strength and thus that this value is most applicable for estimating strength in this region during shock loading.

The HEL defines the lowest threshold for the strength of a material while the WSL defines the limiting stress for elastic behaviour. This transition not only fixes the ultimate strength of solids but stabilises the refractive index of glasses and, as seen above, controls transparency and conductivity thresholds [100, 111, 113]. By such investigations, the transition to homogeneous nucleation can be tracked using shock methods and this work suggests that the ultimate shear strength of new materials might be measured directly using this technique [48]. Finally, the front itself then obeys the Swegle-Grady, fourth power relation, with the work done by the impulse, and the time taken to complete the processes operating, determining its extent [96, 101, 102, 128].

Closure

This review has highlighted the strength of solids across the weak and strong shock regimes and illustrated a critical threshold, the weak shock limit, that separates the two. This threshold divides inhomogeneous from homogeneous states behind a propagating shock. The following conclusions and inferences may be drawn.

(i)   In the weak shock regime, the nature of the driving impulse controls the critical length scales probed by the front and thus the defect distribution in the as-received material fixes the response.

(ii)   Above the WSL, the shear component of the stress applied exceeds the theoretical strength of the material and inelasticity is homogeneously nucleated behind the front.

(iii)   The strength of a material rises from the Hugoniot elastic limit at the start of the weak shock regime to the theoretical strength at the HEL. Beyond the WSL the strength may plateau or, as pulse amplitudes increase, other phase changes such as melting may occur that change the state of the material (e.g. [129, 130]).

(iv)   The WSL is the longitudinal stress who's shear component exceeds the theoretical strength, and that admits a regime of homogeneous flow behind the front. The methods outlined in this article can thus be used to infer the ultimate shear strength of solids.

(v)   Above the WSL, a range of further phenomena are observed such as luminescence, conductivity transitions, absorption, changes in transparency and stabilisation of the refractive index in transparent solids.

(vi)   The WSL may indicate the start of fourth power behaviour in shocked solid phase materials and this implies a constancy of energy and temporal duration through strong shock fronts [96].

Future Perspectives

The observations presented here suggest new frontiers exist at high pressure to explore extreme compressions. In the weak shock regime, better representations of the pre-existing defect structures present in matter can be gained from 5D (positional, elemental, chemical) information, gleaned from new national facility diagnostics (through tomography, diffraction, spectroscopy) [131–138]. This will allow predictive, first principles modelling of the inhomogeneous states accessed in these materials (e.g. [131]) under more extreme conditions. Challenging problems, and the increased availability of extreme environments and advanced numerical techniques, make work in this area as exciting and important as ever.

Declarations

Conflict of interest The author declare that there is no conflict of interest.

References

1. Malvern LE (1969) Introduction to the mechanics of a continuous medium. Prentice-Hall, Englewood Cliffs
2. von Mises R (1913) Mechanik der festen Körper im plastisch-deformablen Zustand. Nachrichten von der Gesellschaft der Wissenschaften zu Göttingen. Mathematisch-Physikalische Klasse 1:582–592
3. Ward JP (1992) Solid mechanics an introduction. Springer, Dordrecht
4. Davison L, Graham RA (1979) Shock compression of solids. Phys Rep 55:255–379
5. Duvall GE, Graham RA (1977) Phase transitions under shock wave loading. Rev Mod Phys 49:523–579
6. Follansbee PS (2014) Fundamentals of strength. Wiley, Hoboken
7. Novikov SA (1981) Shear stress and spall strength of materials under shock loads (review). J Appl Mech Tech Phys 22:385–394
8. Rice RW (1971) The compressive strength of ceramics. Mater Sci Res 5:195–227
9. Vogler TJ (2011) Measuring strength at ultrahigh strain rates. In: Proulx T (ed) Dynamic behavior of materials. Vol. 1: proceedings of the 2010 annual conference on experimental and applied mechanics. Springer, Berlin. p 329–332
10. Vogler TJ, Chhabildas LC (2006) Strength behavior of materials at high pressures. Int J Impact Eng 33:812–825
11. Field JE, Walley SM, Bourne NK, Huntley JM (1994) Experimental methods at high rates of strain. J Phys IV France 4(C8):3–22
12. Field JE, Walley SM, Bourne NK, Huntley JM (1998) Review of experimental techniques for high rate deformation studies. In: Proceedings of the Acoustics and Vibration Asia '98. Acoustics and Vibration Asia 98 Conference, Singapore. p 9–38
13. Walley SM (2010) Historical review of high strain rate and shock properties of ceramics relevant to their application in armour. Adv Appl Ceram 109(8):446–466
14. Bourne NK (2011) Materials' physics in extremes: akrology. Metall Mater Trans A 42A(10):2975–2984
15. Bourne NK (2011) On failure and dynamic performance of materials. In: Proulx T (ed) Dynamic behavior of materials. Vol. 1: proceedings of the 2010 annual conference on experimental and applied mechanics. Springer, Berlin. p 25–30
16. Bourne NK (2015) On the ultimate strength of condensed matter. Metall Mater Trans A 46(10):4498–4505
17. Bourne NK (2015) On strength at yield in condensed matter. Metall Mater Trans A 46(10):4491–4497
18. Ashcroft NW (2009) Pressure for change in metals. Nature 458(7235):158–159
19. Koenig M, Benuzzi-Mounaix A, Ravasio A, Vinci T, Ozaki N, Lepape S, Batani D, Huser G, Hall T, Hicks D, MacKinnon A, Patel P, Park HS, Boehly T, Borghesi M, Kar S, Romagnani L (2005) Progress in the study of warm dense matter. Plasma Phys Control Fusion 47:B441–B449
20. Bourne NK (2013) Materials in mechanical extremes; fundamentals and applications. Cambridge University Press, Cambridge
21. Gray GT III (2012) High-strain-rate deformation: mechanical behavior and deformation substructures induced. Ann Rev Mater Res 42:285–303
22. Fortov VE (2011) Extreme states of matter: on earth and in the cosmos. Elsevier, Amsterdam
23. Kanel GI, Razorenov SV, Baumung K, Singer J (2001) Dynamic yield and tensile strength of aluminum single crystals at temperatures up to the melting point. J Appl Phys 136:3230–3232
24. Bourne NK (2014) The threshold for hydrodynamic behaviour in solids under extreme compression. J Appl Phys 116(9):093505
25. Gray GT III, Maudlin PJ, Hull LM, Zuo K, Chen S-R (2005) Predicting material strength, damage, and fracture: the synergy between experiment and modeling. Los Alamos Sci 29:81–93
26. Richter G, Hillerich K, Gianola DS, Mönig R, Kraft O, Volkert CA (2009) Ultrahigh strength single crystalline nanowhiskers grown by physical vapor deposition. Nano Lett 9:3048–3052
27. Hopkinson B (1914) A method of measuring the pressure produced in the detonation of high explosives or by the impact of bullets. Proc R Soc Lond A 89:411–413
28. Gray GT III (200) Shock wave testing of ductile materials. In: Kuhn H, Medlin D (eds) ASM Handbook. Vol. 8: mechanical testing and evaluation. ASM International, Materials Park, OH. p 530–538
29. Remington BA, Allen P, Bringa EM, Hawreliak J, Ho D, Lorenz KT, Lorenzana H, McNaney JM, Meyers MA, Pollaine SW, Rosolankova K, Sadik B, Schneider MS, Swift D, Wark J, Yaakobi B (2006) Material dynamics under extreme conditions of pressure and strain rate. Mater Sci Technol 22:474–488
30. Alexander CS (2012) Dynamic material strength measurement utilizing magnetically applied pressure-shear. EPJ Web Conf 26:01043
31. Asay JR, Ao T, Vogler TJ, Davis J-P, Gray GT III (2009) Yield strength of tantalum for shockless compression to 18 GPa. J Appl Phys 106:073515
32. Ashuach Y, Rosenberg Z, Dekel E, Ginzburg A (2006) More on the strength of materials under high shock pressures. In: Furnish MD, Elert M, Russell TP, White CT (eds) Shock compression of condensed matter—2005. American Institute of Physics, Melville, NY, pp 1241–1244
33. Gray GT III, Bourne NK, Millett JCF (2003) Plate impact response of tantalum: lateral stress and shear strength through the front. J Appl Phys 94:6430–6436
34. Smallman RE, Bishop RJ (1999) Modern physical metallurgy and materials engineering (sixth edition). Elsevier, Amsterdam
35. Paxton AT, Gumbsch P, Methfessel M (1991) A quantum mechanical calculation of the theoretical strength of metals. Philos Mag Lett 63:267–274
36. Pokluda J, Cerny M, Sandera P, Sob M (2004) Calculations of theoretical strength: state of the art and history. J Comput Aided Mater Des 11:1–28
37. Duffy TS (2007) Strength of materials under static loading in the diamond anvil cell. In: Furnish MD, Elert ML, Russell TP, White CT (eds) Shock compression of condensed matter—2007. AIP, New York, pp 639–644
38. He D, Duffy TS (2006) X-ray diffraction study of the static strength of tungsten to 60 GPa. Phys Rev B 73:134106
39. Kelly A (1973) Strong solids, 2nd edn. Clarendon Press, Oxford
40. Orowan E (1949) Fracture and strength of solids. Rep Progr Phys 12:185–232
41. Orowan E (1934) Zur Kristallplastizität. II - Die dynamische Auffassung der Kristallplastizität Zeitschrift FüR Physik. Z Phys 89:614–633
42. Frenkel J (1926) Zur Theorie der Elastizitätsgrenze und der Festigkeit kristallinischer Körper. Z Phys 37:572–609
43. Petch NJ (1953) The cleavage strength of polycrystals. J Iron Steel Inst Lond 173:25–28
44. Ruoff AL (1978) On the ultimate yield strength of solids. J Appl Phys 49:197–200
45. Moriarty JA, Benedict L, Glosli J, Hood R, Orlikowski D, Patel M, Söderlind P, Streitz F, Tang M, Yang L (2006) Robust quantum-based interatomic potentials for multiscale modeling in transition metals. J Mater Res 21:563

46. Xu W, Moriarty JA (1996) Atomistic simulation of ideal shear strength, point defects, and screw dislocations in bcc transition metals: Mo as a prototype. Phys Rev B 54(10):6941–6951

47. Moriarty JA, Xu W, Soderlind P, Belak J, Yang LH, Zhu J (1999) Atomistic simulations for multiscale modeling in bcc metals. J Eng Mater Technol Trans ASME 121(2):120–125

48. Gurrutxaga-Lerma B, Balint DS, Dini D, Eakins DE, Sutton AP (2015) The role of homogeneous nucleation in planar dynamic discrete dislocation plasticity. J Appl Mech 82(7):071008

49. Roundy D, Krenn C, Cohen M, Morris J Jr (1999) Ideal shear strengths of fcc aluminum and copper. Phys Rev Lett 82(13):2713–2716

50. Luo W, Roundy D, Cohen M, Morris J Jr (2002) Ideal strength of bcc molybdenum and niobium. Phys Rev B 66(9):094110

51. Krenn CR, Roundy D, Cohen ML, Chrzan DC, Morris JW Jr (2002) Connecting atomistic and experimental estimates of ideal strength. Phys Rev B 65:134111

52. Söderlind P, Moriarty JA (1998) First-principles theory of Ta up to 10 Mbar pressure: structural and mechanical properties. Phys Rev B 57(10):10340

53. Follansbee PS, Regazzoni G, Kocks UF (1984) The transition in drag-controlled deformation in copper at high strain rates. Inst Phys Conf Ser 70:71–80

54. Graham RA, Brooks WP (1971) Shock-wave compression of sapphire from 15 to 420 kbar: the effects of large anisotropic compressions. J Phys Chem Solids 32:2311

55. Bourne NK, Millett JCF, Chen M, McCauley JW, Dandekar DP (2007) On the Hugoniot elastic limit in polycrystalline alumina. J Appl Phys 102:073514

56. Whitley VH, McGrane SD, Eakins DE, Bolme CA, Moore DS, Bingert JF (2011) The elastic-plastic response of aluminum films to ultrafast laser-generated shocks. J Appl Phys 109:013505

57. Gupta YM, Winey JM, Trivedi PB, LaLone BM, Smith RF, Eggert JH, Collins GW (2009) Large elastic wave amplitude and attenuation in shocked pure aluminum. J Appl Phys 105(3):036107

58. Ashitkov SI, Agranat MB, Kanel GI, Komarov PS, Fortov VE (2010) Behavior of aluminum near an ultimate theoretical strength in experiments with femtosecond laser pulses. JETP Lett 92:516–520

59. Rothman SD, Bandyopadhyay S, Brown CRD, George AA, Gjsh-chkhmyj N, Greedharee RSR, Guymer TM, Park N, Parsley MC, Price E, Turner JG (2009) Laser-driven spall; velocity interfer-ometry and target recovery. In: Elert ML, Buttler WT, Furnish MD (eds) 16th conference of the American-Physical-Society-Topical-Group on shock compression of condensed matter. AIP Conference Proceedings, Nashville, TN. p 961–965

60. Moshe E, Eliezer S, Henis Z, Werdiger M, Dekel E, Horovitz Y, Maman S, Goldberg IB, Eliezer D (2000) Experimental measurements of the strength of metals approaching the theo-retical limit predicted by the equation of state. Appl Phys Lett 78(12):1555–1557

61. Meyers M, Jarmakani H, Bringa E, Remington B (2009) Dislocations in shock compression and release. In: Hirth J, Kubin L (eds) Dislocations in solids. Elsevier, Amsterdam, North Holland, pp 94–197

62. Hirth J, Lothe J (1982) Theory of dislocations, 2nd edn. Wiley, New York

63. Appleby-Thomas GJ, Hazell PJ (2010) A study on the strength of an armour-grade aluminum under high strain-rate loading. J Appl Phys 107:123508

64. Asay JR, Ao T, Davis J-P, Hall C, Vogler TJ, Gray GT III (2008) Effect of initial properties on the flow strength of aluminum dur-ing quasi-isentropic compression. J Appl Phys 103:083514

65. Bat'kov YV, Knyazev VN, Novikov SA, Rayevskii VA, Fishman ND (1999) Shear strength of aluminum upon shockless compres-sion. Combust Explos Shock Waves 35:707–710

66. Bonora N, Bourne NK, Garcea SC, Ruggiero A, Gentile D, Ian-nitti F, Testa G (2018) Numerical simulation and validation of damage in AA1100 Aluminum Symmetric Taylor Impact (ROR). In: Chau R, Germann TC, Sewell TD (eds) Shock compression of condensed matter 2017. AIP, Melville, NY, p 070006

67. Huang H, Asay JR (2005) Compressive strength measurements in aluminum for shock compression over the stress range of 4–22 GPa. J Appl Phys 98:033524

68. Lipkin J, Asay JR (1977) Reshock and release of shock-com-pressed 6061–T6 aluminum. J Appl Phys 48:182–189

69. Vogler TJ, Ao T, Asay JR (2009) High-pressure strength of alu-minum under quasi-isentropic loading. Int J Plast 25:671–694

70. Barton NR, Bernier JV, Becker R, Arsenlis A, Cavallo R, Marian J, Rhee M, Park HS, Remington BA, Olson RT (2011) A multi-scale strength model for extreme loading conditions. J Appl Phys 109:073501

71. Bronkhorst CA, Gray GT III, Addessio FL, Livescu V, Bourne NK, McDonald SA, Withers PJ (2016) Response and representa-tion of ductile damage under varying shock loading conditions in tantalum. J Appl Phys 119:085103

72. Millett JCF, Whiteman G, Park NT, Case S, Bourne NK (2013) The role of cold work on the shock response of tantalum. J Appl Phys 113(23):233502

73. Murphy WJ, Higginbotham A, Kimminau G, Barbrel B, Bringa EM, Hawreliak J, Kodama R, Koenig M, McBarron W, Mey-ers MA, Nagler B, Ozaki N, Park N, Remington B, Rothman S, Vinko SM, Whitcher T, Wark JS (2010) The strength of single crystal copper under uniaxial shock compression at 100 GPa. J Phys Condens Matter 22:065404

74. Bourne NK, Gray GT III, Millett JCF (2009) On the shock response of cubic metals. J Appl Phys 106(9):091301

75. Bourne NK, Jones D, Fensin S, Trujillo C, Martinez D, Gray GT III (2018) On the dynamic tensile strength of an FCC metal. In: Chau R, Germann TC, Sewell TD (eds) Shock compression of condensed matter 2017. AIP, Melville, NY, p 070007

76. Bourne NK, Millett JCF (2000) On impact upon brittle solids. J Phys IV 10:281–286

77. Bourne NK, Millett JCF, Rosenberg Z, Murray NH (1998) On the shock induced failure of brittle solids. J Mech Phys Solids 46:1887–1908

78. Millett J, Bourne N (2000) The shear strength of a shocked borosilicate glass with an internal interface. Scripta Mater 42:681–685

79. Murray NH, Bourne NK, Rosenberg Z (1998) The dynamic compressive strength of aluminas. J Appl Phys 84:4866–4871

80. Rosenberg Z (1994) On the shear strength of shock loaded brittle solids. J Appl Phys 76:1543–1546

81. Rosenberg Z, Bless SJ (1986) Determination of dynamic yield strengths with embedded manganin gages in plate-impact and long-rod experiments. Exp Mech 26:279–282

82. Bourne NK, Gray GT III, Millett JCF (2003) On the dynamic response of four polymers. J Phys IV France 110:815–820

83. Bourne NK, Millett JCF (2003) The high-rate response of an elastomer. Proc R Soc Lond A 459:567–576

84. Bourne NK, Millett JCF, Barnes N, Belcher I (2002) The devi-atoric response of an epoxy resin to one-dimensional shock loading. In: Furnish MD, Thadhani NN, Horie Y (eds) Shock compression of condensed matter—2001. American Institute of Physics, Melville, NY, pp 649–652

85. Bourne NK, Millett JCF, Gray GT III, Mort P (2002) On the strength behaviour of Kel-F-800 and estane polymers. In: Fur-nish MD, Thadhani NN, Horie Y (eds) Shock compression

of condensed matter—2001. American Institute of Physics, Melville, NY, pp 653–656

86. Millett JCF, Bourne NK (2000) The deviatoric response of PMMA to one-dimensional shock loading. J Appl Phys 88:7037–7040

87. Millett JCF, Bourne NK (2001) Shock response of the elastomer polychloroprene. J Appl Phys 89:2576–2579

88. Millett JCF, Bourne NK (2006) The shock induced equation of state and shear strength of PVDF. J Phys IV France 134:719–724

89. Millett JCF, Bourne NK, Barnes NR (2002) The behavior of an epoxy resin under one-dimensional shock loading. J Appl Phys 92:6590–6594

90. Millett JCF, Bourne NK, Brown EN, Gray GT III (2007) Shear strength and its variation according to structure in shock loaded polyethylene. In: Elert M, Furnish MD, Chau R, Holmes N, Nguyen J (eds) Shock compression of condensed matter—2007. American Institute of Physics, Melville, NY, pp 719–722

91. Millett JCF, Gray GT III, Bourne NK (2004) Longitudinal and lateral stress measurements in shock loaded PEEK. In: Furnish MD, Gupta YM, Forbes JW (eds) Shock compression of condensed matter—2003. American Institute of Physics, Melville, NY, pp 663–666

92. Millett JCF, Whiteman G, Stirk SM, Bourne NK (2011) Shear strength measurements in a shock loaded commercial silastomer. J Phys D 44:185403

93. Tan H, Dai CD, Zhang LY, Xu CH (2005) Method to determine the melting temperatures of metals under megabar shock pressures. Appl Phys Lett 87:221905

94. Jensen BJ, Cherne FJ, Cooley JC, Zhernokletov MV, Kovalev AE (2010) Shock melting of cerium. Phys Rev B 81:214109

95. Nguyen JH, Holmes NC (2004) Melting of iron at the physical conditions of the Earth's core. Nature 427:339–342

96. Grady DE (2010) Structured shock waves and the fourth-power law. J Appl Phys 107:013506

97. Bushman AV, Lomonosov IV, Khishchenko KV (2002) Rusbank Shock Wave Database. http://www.ihed.ras.ru/rusbank/

98. Marsh SP (1980) Shock Hugoniot Data. University of California Press, Berkeley, CA

99. van Thiel M (1966) Compendium of shock wave data. Lawrence Radiation Laboratory, Livermore, CA

100. Greaves GN, Greer AL, Lakes RS, Lakes RS, Rouxel T (2011) Poisson's ratio and modern materials. Nat Mater 10(11):823–837

101. Swegle JW, Grady DE (1985) Shock viscosity and the prediction of shock wave rise times. J Appl Phys 58:692–701

102. Grady DE (2015) Unifying role of dissipative action in the dynamic failure of solids. J Appl Phys 117(16):165905

103. Tschopp M, McDowell D (2008) Influence of single crystal orientation on homogeneous dislocation nucleation under uniaxial loading. J Mech Phys Solids 56(5):1806–1830

104. Dremin AN, Adadurov GA (1964) Behaviour of a glass at dynamic loading. Fiz Tverd Tela 6(6):1757–1764

105. Lakshtanov DL, Stanislav A, Sinogeikin V, Bass JD (2007) High-temperature phase transitions and elasticity of silica polymorphs. Phys Chem Min 34:11–22

106. Bless SJ, Brar NS, Rosenberg Z (1988) Strength of soda lime glass under shock compression. In: Schmidt SC, Holmes NC (eds) Shock waves in condensed matter 1987. Elsevier, Amsterdam, North Holland, pp 309–312

107. Bourne NK, Millett JCF, Rosenberg Z (1997) On the origin of failure waves in glass. J Appl Phys 81:6670–6674

108. Gibbons RV, Ahrens TJ (1971) Shock metamorphism of silicate glasses. J Geophys Res 76:5489–5498

109. Kanel GI, Rasorenov SV, Fortov VE, Abasehov MM (1991) The fracture of glass under high pressure impulsive loading. High Press Res 6:225–232

110. Brar NS, Bless SJ (1992) Failure waves in glass under dynamic compression. High Pressure Res 10(5–6):773–784

111. Renganathan P, Toyoda Y, Gupta YM (2020) Optical response of soda-lime glass shocked to 14 GPa. J Dyn Behav Mater 6:207–212

112. Davis MJ (2016) Laser-shock-induced spall and the intrinsic strength of glass. Int J Appl Glas Sci 7(3):364–373

113. Alexander CS (2009) Index of refraction of shock loaded soda-lime glass. In: Furnish MD, Elert M, Chau R (eds) Shock compression of condensed matter 2009. American Institute of Physics, College Park, pp 1431–1434

114. Erskine DJ, Nellis WJ (1991) Shock-induced martensitic phase transformation of graphite to diamond. Nature 349:417–319

115. Erskine DJ, Nellis WJ (1992) Shock-induced martensitic transformation of highly oriented graphite to diamond. J Appl Phys 71:4882–4886

116. Bless SJ, Bourne NK (2004) The effect of shock rise time on strength of alumina in 1D stress and 1D strain. In: Furnish MD, Gupta YM, Forbes JW (eds) Shock compression of condensed matter—2003. American Institute of Physics, Melville, NY, pp 711–714

117. Bourne NK, Green WH, Dandekar DP (2006) On the one-dimensional recovery and microstructural evaluation of shocked alumina. Proc R Soc A 462:3197–3212

118. Chen MW, McAuley JW, Dandekar DP, Bourne NK (2006) Dynamic plasticity and failure of high-purity alumina under shock loading. Nat Mater 5:814–818

119. Reinhart WD, Chhabildas LC (2003) Strength properties of Coors AD995 alumina in the shocked state. Int J Impact Eng 29:601–619

120. Grady DE (2015) Hugoniot equation of state and dynamic strength of boron carbide. J Appl Phys 117:165904

121. Kanel GI, Nellis WJ, Savinykh AS, Razorenov SV, Rajendran AM (2009) Response of seven crystallographic orientations of sapphire crystals to shock stresses of 16–86 GPa. J Appl Phys 106(4):043524

122. Lankford J (2004) The role of dynamic material properties in the performance of ceramic armour. Int J Appl Ceram Technol 1:205–210

123. Erskine D (1994) High pressure Hugoniot of sapphire. In: Schmidt SC, Dandekar, DP, Forbes JW (eds) High-pressure science and technology—1993. AIP Press, New York, pp 141–143

124. Reinhart WD, Chhabildas LC, Vogler TJ (2006) Investigating phase transitions and strength in single-crystal sapphire using shock–reshock loading techniques. Int J Impact Eng 33:655–669

125. Duvall GE (1964) Propagation of plane shock waves in a stress-relaxing medium. In: Kolsky H, Prager W (eds) Stress waves in anelastic solids. Springer-Verlag, Berlin, pp 20–32

126. Urtiew PA (1974) Effect of shock loading on transparency of sapphire crystals. J Appl Phys 45:3490

127. Weir ST, Mitchell AC, Nellis WJ (1996) Electrical resistivity of single-crystal Al_2O_3 shock-compressed in the pressure range 91–220 GPa (0.91–2.20 Mbar). J Appl Phys 80:1522

128. Grady DE (2018) Principles underlying the fourth power nature of structured shock waves. In: Shock compression of condensed matter. AIP Conference Proceedings, St Louis, MO. p 070014

129. Kanel GI (2014) Unusual behaviour of usual materials in shock waves. J Phys Conf Ser 500:012001

130. Kanel GI, Fortov VE, Razorenov SV (2004) Yield and strength properties of metals and alloys at elevated temperatures. Shock-wave phenomena and the properties of condensed matter. Springer-Verlag, New York, pp 83–109

131. Miller MP, Pagan DC, Beaudoin AJ, Nygren KE, Shadle SJ (2020) Understanding micromechanical material behavior using synchrotron X-rays and in situ loading. Metall Mater Trans A 51A:4360–4376

132. https://lansce.lanl.gov/facilities/pRad/
133. https://www.diamond.ac.uk/
134. https://www.isis.stfc.ac.uk/
135. https://www.esrf.eu
136. https://www.aps.anl.gov

137. https://www.xfel.eu
138. https://lcls.slac.stanford.edu